

See discussions, stats, and author profiles for this publication at: <https://www.researchgate.net/publication/236607045>

A Multi-Scale Soil Moisture and Freeze-Thaw Monitoring Network on the Third Pole

Article in *Bulletin of the American Meteorological Society* · December 2013

DOI: 10.1175/BAMS-D-12-00203.1

CITATIONS

106

READS

403

12 authors, including:



Kun Yang

Tsinghua University

180 PUBLICATIONS 5,856 CITATIONS

[SEE PROFILE](#)



Jun Qin

Institute of Tibetan Plateau Research Chinese Academy of Sciences

84 PUBLICATIONS 3,110 CITATIONS

[SEE PROFILE](#)



Long Zhao

Southwest University in Chongqing

23 PUBLICATIONS 629 CITATIONS

[SEE PROFILE](#)



Yingying Chen

Chinese Academy of Sciences

43 PUBLICATIONS 1,378 CITATIONS

[SEE PROFILE](#)

Some of the authors of this publication are also working on these related projects:



Multi-sensor Land Data Assimilation and Its Role in Hydroclimate Prediction [View project](#)



Soil moisture and data assimilation [View project](#)

A MULTISCALE SOIL MOISTURE AND FREEZE–THAW MONITORING NETWORK ON THE THIRD POLE

BY KUN YANG, JUN QIN, LONG ZHAO, YINGYING CHEN, WENJUN TANG, MENGLI HAN, LAZHU, ZHUOQI CHEN, NING LV, BAOHONG DING, HUI WU, AND CHANGGUI LIN

A multiscale soil moisture and temperature monitoring network was established on the central Tibetan Plateau to support remote sensing, land hydrological modeling, and surface process studies.

SCIENTIFIC BACKGROUND AND OBJECTIVES. As the highest plateau in the world, the Tibetan Plateau (TP) directly impacts its surrounding climate and environment through atmospheric and hydrological processes. Meanwhile, the TP climate changed significantly (such as rapid warming, moistening, solar dimming, and wind stilling) over the past 30 years (Yang et al. 2011), which further altered its environment (e.g., glacier retreat, lake expansion, and permafrost degradation, etc.) and brought environmental risks and disasters to the plateau's surrounding regions. The “third pole” was proposed as a geographic element to cover the TP and its adjacent mountains (Qiu 2008), and the “Third Pole Environment” (TPE) was then launched as an international program in 2009, with intension to pool international efforts to reveal and quantify the “water–ice–air–ecosystem–human” interactions in this region (Yao et al. 2012). Among the multisphere interactions on the TP, soil moisture (SM) plays a fundamental role in controlling land surface energy partition, adjusting surface runoff and soil drainage, regulating canopy transpiration and carbon

AFFILIATIONS: YANG, QIN, Y. CHEN, AND TANG—Key Laboratory of Tibetan Environment Changes and Land Surface Processes, Institute of Tibetan Plateau Research, Chinese Academy of Sciences, Beijing, China; ZHAO, HAN, LAZHU, DING, WU, AND LIN—Key Laboratory of Tibetan Environment Changes and Land Surface Processes, Institute of Tibetan Plateau Research, Chinese Academy of Sciences, and University of Chinese Academy of Sciences, Beijing, China; Z. CHEN—College of Global Change and Earth System Science, Beijing Normal University, Beijing, China; LV—State Key Laboratory of Resources and Environmental Information System, Institute of Geographic Sciences and Natural Resources Research, Chinese Academy of Sciences, Beijing, China

CORRESPONDING AUTHOR: Kun Yang, Institute of Tibetan Plateau Research, Chinese Academy of Sciences, Bldg. 3, Courtyard 16, Lincui Rd., Chaoyang District, Beijing 100101, China
E-mail: yangk@itpcas.ac.cn

The abstract for this article can be found in this issue, following the table of contents.

DOI:10.1175/BAMS-D-12-00203.1

A supplement to this article is available online (10.1175/BAMS-D-12-00203.2)

In final form 20 April 2013
©2013 American Meteorological Society

assimilation, and modulating soil freeze–thaw status. Therefore, SM is a commonly measured parameter in a series of recent and ongoing field experiments associated with the energy and water cycle of the Asian monsoon, hydrological processes, ecosystem adaptation, and cryosphere changes over the TP (Xu et al. 2008; Ma et al. 2008; Zhang et al. 2012). Nevertheless, these measurements are scarce relative to the broad area of the third pole.

To facilitate process studies at a regional scale, land modeling and satellite remote sensing are intended to provide regional SM. For instance, the Global Land Data Assimilation System (Rodell et al. 2004) provides simulated SM data at 1.0° and 0.25° resolution. Remote sensing retrievals from the Advanced Microwave Scanning Radiometer (AMSR-E) (Kawanishi et al. 2003), the Soil Moisture and Ocean Salinity (SMOS) mission (Kerr et al. 2001), *MetOp-A* Advanced Scatterometer (ASCAT) (Bartalis et al. 2007), and the upcoming Soil Moisture Active Passive (SMAP) mission (Entekhabi et al. 2010) estimate SM data at a resolution of tens of kilometers. The SM product from SMAP active signals will have a resolution of 9 km. These approaches need calibration and validation against ground truth. Because of the high spatial variability of SM, the ground truth at a satellite pixel or model grid size cannot be obtained through measurements at a single station. Instead, many efforts were made to develop measuring networks to obtain the SM ground truth at specific spatial scales. The International Soil Moisture Network (ISMN; Dorigo et al. 2011) was initiated to pool in situ SM networks worldwide in cooperation with the Global Soil Moisture Data Bank developed by Robock et al. (2000).

Over the past two decades, many efforts have been specifically dedicated to estimating regional SM on the TP through microwave remote sensing (e.g., Fujii and Koike 2001; Wen et al. 2003; van der Velde et al. 2012), land data assimilation (e.g., K. Yang et al. 2007; Rasmy et al. 2011; Lu et al. 2012), and land surface modeling (e.g., Gao et al. 2004; Yang et al. 2005). Moreover, the TP represents an extreme environment under which it is easy to identify the applicability of a SM product. Su et al. (2011) developed a SM observatory on the TP, which consists of three networks located in distinct climate regimes: 20 stations in a cold and arid area, 20 stations in a cold and humid area, and 5 stations in a cold and semiarid area. They found that several satellite SM products are comparable to the ground observations in the arid area and the humid area but biased by 0.2–0.3 m³ m⁻³ in the semiarid area. These large biases were not reported in

previous studies, showing great challenges to improve SM products in this semiarid area.

In addition, the soil freeze–thaw (F/T) is a typical process on the TP. It imposes effects on soil hydrology and vegetation growth as well as the bedrock stability of the plateau highway and railway. Many efforts have made to estimate the F/T state through remote sensing (e.g., Zhang and Armstrong 2001; Jin et al. 2009; Zhao et al. 2011; Li et al. 2012) and land surface modeling (e.g., Li and Koike 2003; Oelke and Zhang 2007). Again, these approaches also need validations under the plateau environment.

In this paper, we present a multiscale Soil Moisture and Temperature Monitoring Network on the central TP (CTP-SMTMN), which is located in a cold and semiarid area with an average elevation above 4500 m above mean sea level (MSL) (see details in “Experimental area” section). The network was accomplished in June 2012 after 3 years of construction under the harsh environment. It consists of 56 stations that measure soil moisture and temperature at three spatial scales (see details in “Network configuration” section). The network was designed to fulfill the three objectives below.

First, the network can provide ground truth of SM and soil F/T state at three spatial scales so that it can be used to calibrate/evaluate SM and F/T estimates from microwave remote sensing, land data assimilation, and land hydrological modeling at a variety of spatial scales. SM and F/T state retrieved from microwave remote sensing are often contaminated by dense biomass. Our experimental area has a high soil moisture dynamic range (owing to monsoonal precipitation in summer) but a low biomass (owing to low temperature and short growing period), making it possible to separate the impact of soil moisture and vegetation on microwave signals. In this sense, this area is an ideal place for calibrating/evaluating microwave SM algorithms. It is worth pointing out that our experimental area is collocated with but larger than the semiarid experimental area in Su et al. (2011). The new network enhances the function of this area as a calibration/validation site for satellite SM retrievals.

Second, the network can provide data for soil moisture scaling studies. SM has high spatial variability, and its spatial scaling is a key and fundamental issue for a number of purposes. Most of existing networks provide either dense measurements at small scales (several kilometers) or sparse measurements at a large scale (~100 km), and this situation is not favorable for soil moisture upscaling/downscaling analyses. Our network measures SM at three spatial scales that are often concerned in hydrometeorological studies,

and thus it provides a unique opportunity to evaluate existing spatial scaling methods and to develop new methods. In addition, the data are recorded at a high temporal resolution (~30 min) and can be used for studies of SM temporal variability and scaling.

Third, the network complements the existing hydrometeorological observations in this area. To investigate the plateau land–atmosphere interactions, some hydrometeorological instruments (such as weather station, wind profiler, and flux tower) have been deployed in the experimental area through field campaigns of the Global Energy and Water Cycle Experiment (GEWEX) and Coordinated Enhanced Observing Period (CEOP) as well as follow-on projects (Ma et al. 2008), but SM measurements are still sparse in space and only applicable to point-scale process studies. Our network provides dense measurement of both soil moisture and soil temperature. Also, we measure soil texture and organic matter content at each station through laboratory analyses. The network and the ancillary data can

support the study of water–ice–air–ecosystem interactions at different scales.

EXPERIMENTAL AREA. As shown in Fig. 1, our network is located within an area of 10,000 km² in the central Tibetan Plateau. Despite significant relief in some parts, this area is fairly smooth with rolling hills.

This area is influenced by the South Asian summer monsoon. Annual precipitation amount is about 400–500 mm in most of the central TP, and three quarters of precipitation occurs during the monsoon season [June–August (JJA)]. The land surface is dry

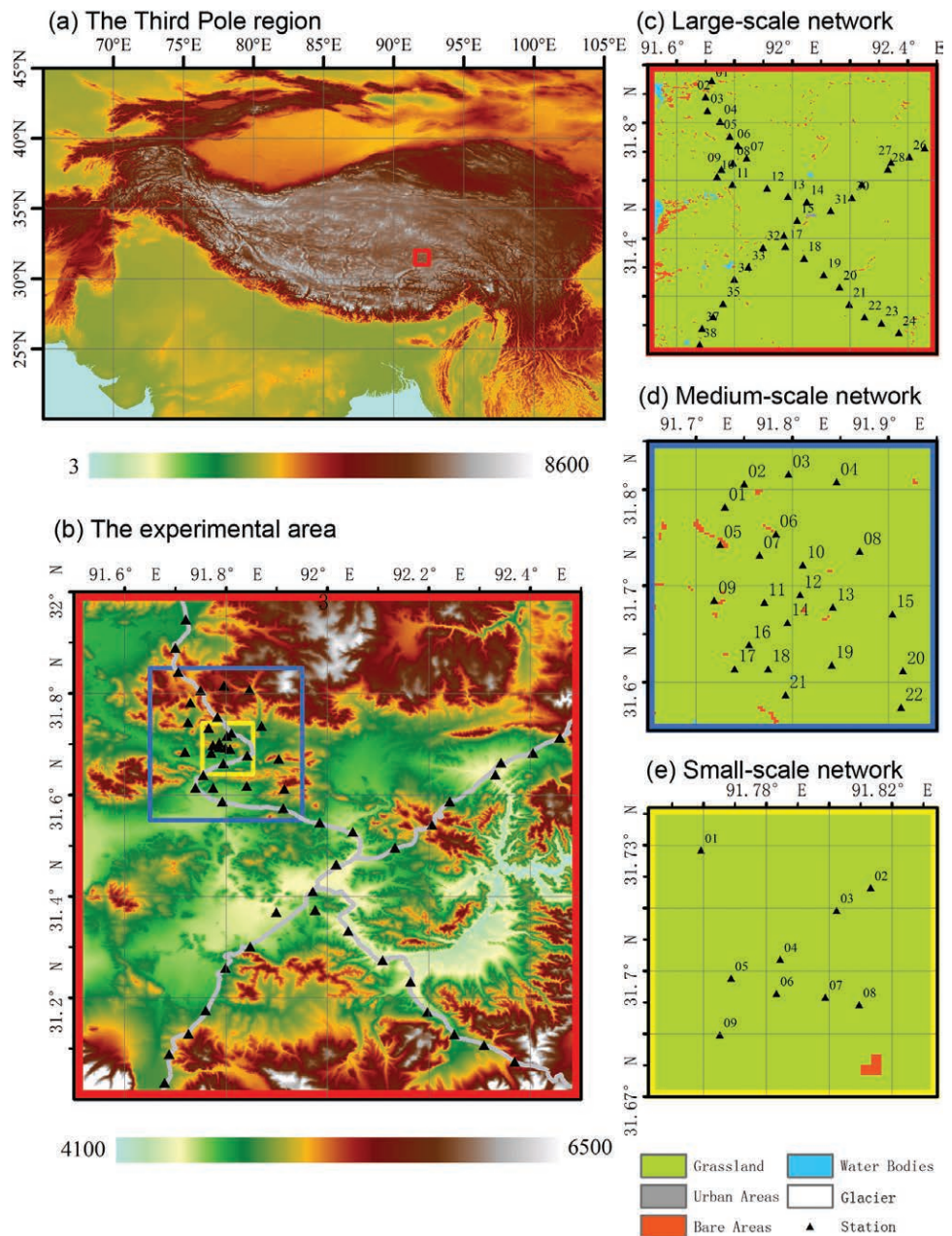


FIG. 1. The configuration of the CTP-SMTMN: (a) network position (denoted by the small rectangle) on the central Tibetan Plateau, (b) the experimental area and station locations (the gray curves are the national/provincial roads), and (c)–(e) the large, medium, and small networks. Elevation is shown in (a),(b) and land use is shown in (c)–(e).

from December to April; after the onset of the monsoon (about the end of May to the middle of June), the surface gradually moistens owing to frequent rainfall events. The soil surface starts its diurnal F/T cycle since October and becomes fully frozen during December–February. Therefore, surface SM has high seasonal dynamic range: low in the premonsoon season, high in the monsoon season, and partially iced in the frozen season. The SM diurnal range is also high during the diurnal F/T cycle period, with high content during days and low content during nights (M. Yang et al. 2007).

The land surfaces in the experimental area are typically characterized by alpine grasslands (93.46% of the area), as seen in Fig. 1. Because of its high elevation and low temperature, the growing season of the alpine grasses is short (~3 months), and the grass height is several centimeters. The intraannual MODIS normalized difference vegetation index (NDVI) ranges over 0.15–0.51, indicating a low biomass. Other land cover types are bare soil (3.61%), waters (1.57%), urban (0.69%), and glacier (0.67%). Water bodies are mainly located near the west edge of the area, and the urban area (Naqu city) lies in the center of this area.

Regarding soil texture in this area, silt and sand are dominant components with a comparable magnitude (around 50% and 46% on average, respectively), while clay content consistently maintains at a low value less than 10%. Soil texture components show notable spatial variability (about 13% and 20% for mass percent of silt and sand, respectively). Another typical feature is that soil organic carbon (SOC) content is generally high in the topsoil (averagely 3.6% in mass) and gradually decreases with soil depth (around 0.6% at depth of 40 cm) (Chen et al. 2012). Soils with high SOC contents have high porosity and high water retention capacity, whereas soils with low SOC contents have opposite soil properties. The variability in soil texture and SOC leads to strong SM heterogeneity in both horizontal and vertical extensions, which significantly affects surface energy budget and ecological/hydrological processes.

Despite the harsh environment for construction and maintenance of ground observations, this area is a favorable place for microwave remote sensing of soil moisture. First, this area has low biomass, leading to weak attenuation of microwave signals. Second, the atmospheric absorption and scattering in low-frequency microwave bands are small, owing to both low air mass and air moisture. According to GPS data, the amount of precipitable water hardly exceeds 20 mm in summer and less in other seasons (Liu et al. 2005). Third, radio frequency interference (RFI) for

C-band of AMSR-E is severe in many regions in the world but it is rare in this area. Also, the RFI for SMOS L-band is severe in eastern China, but the situation is much better for the TP and there are enough retrieved data to show seasonal variations of SM.

NETWORK CONFIGURATION. *Site deployment at triple scales.* The CTP-SMTMN has been accomplished through three field campaigns during the summers of 2010–12. Figure 1 shows the deployment of the network. There is a total of 56 stations: 30 stations have started working since August 2010, 20 stations have started working since June 2011, and 6 stations have started working since June 2012. The elevation averaged over the stations is 4650 m MSL. Soil moisture and temperature are measured at three cascaded networks, termed “large network,” “medium network,” and “small network,” with a spatial extent of 1.0°, 0.3°, and 0.1°, respectively. They are designed to match different scales of land hydrological modeling, C-band and L-band passive microwave retrievals (e.g., AMSR-E and SMOS), and active microwave retrievals (e.g., ASCAT and SMAP). The large network has 38 stations, which are deployed along a cross transect (Fig. 1c). The medium network is nested in the large one and consists of 22 stations, which are distributed as uniformly as possible with consideration of logistics. The small network is further nested in the medium grid and consists of nine stations, and it is supposed to be further improved in the future. All stations are deployed on grasslands—the dominant land cover. To improve the representativeness of soil moisture measurements, we have taken into consideration microscale factors, including elevation, slope, aspect, topsoil texture, and SOC content. Table ES1 in the supplement (available online at <http://dx.doi.org/10.1175/BAMS-D-12-00203.2>) lists the geographic location and these parameters for each station. In addition, wetland is not covered by the network because of the high maintenance cost, and we consider its contribution to regional SM through spatial upscaling.

Installation and maintenance. At each station, soil moisture and temperature profiles are measured by four sensors. One sensor is obliquely inserted into 0–5 cm topsoil to measure the averaged near-surface soil moisture and temperature. This depth is comparable to that penetrated by ongoing and upcoming passive microwave sensors. The other three sensors are horizontally inserted at 10-, 20-, and 40-cm depths, respectively. The data are recorded every 30 min, and each record reflects the average of soil moisture and

temperature over the past half hour. The power is supplied by five dry batteries, which can support the measurement for more than 1 year.

The harsh plateau environment is one big challenge to construct the network, and maintaining the network is even more critical. Initially, the datalogger is designed to be hanged on a fixed pillar such that it is easy to operate the whole measuring system. Our experimental area bears a lot of livestock (e.g., yaks and sheep), which may destroy the measuring system. To protect the datalogger, we put it in a container and bury the container in soil. We have designed a cheap waterproof device (see Fig. ES1 in supplement) so as to prevent the logger from being flooded by soil water intrusion into the container. Such a device proves successful, and no datalogger has been damaged by soil water intrusion. Nevertheless, a sensor might stop operation because of natural aging and damage by rats; we expect to renew the sensors at a rate of 10% per year.

We download data manually and check the network's status twice a year—that is, at the beginning of June (when the deep soil is already thawed) and the end of September (before the soil starts freezing), respectively. Note that it is risky to send the measured data via wireless transmission network, considering possible damages of the transmitter by livestock.

Sensor calibration. To establish the monitoring network, we used both the EC-TM and 5TM capacitance probes manufactured by Decagon, United States (www.decagon.com). The sensors measure SM according to the sensitivity of soil dielectric permittivity to liquid soil water. Table ES2 in the supplement shows the specification of the sensor. The sensors can simultaneously measure volumetric water content (VWC) and soil temperature with an accuracy of $\pm 2\%$ VWC and $\pm 1^\circ\text{C}$ and resolution of 0.1% VWC and 0.1°C for mineral soil. However, medium specific calibration is a precondition to guarantee the measuring accuracy of SM; this is particularly important for our experimental area, where high SOC contents in the topsoil may change the relationship between soil dielectric permittivity and liquid soil water (Jacobsen and Schjønning 1993).

To calibrate the sensor, we take 10 undisturbed soil samples from different stations. The soil samples are saturated and then gradually dried through laboratory experiments; during this process, SM is measured by the gravimetric method, and the soil dielectric permittivity is measured by the sensor simultaneously. A calibrated conversion between the measured SM and the measured dielectric permittivity is then developed to account for the impact of SOC content (Fig. 2a). To apply the calibration for our network, we have analyzed the soil texture and SOC content at each measuring depth of each station (see Table ES1 in the supplement for topsoil texture and SOC content data). Figure 2b shows an example to explain the effectiveness of the calibration. The measured SM values before calibration can be negative for the frozen period and thus unreasonable, but they turn to be in the physical range after the calibration, indicating this calibration is indispensable for our network.

PRELIMINARY ANALYSES AND APPLICATIONS. *Observed temperature and moisture variations.* Figure 3a shows the seasonal change of observed daily-mean soil temperature in the 0–5-cm

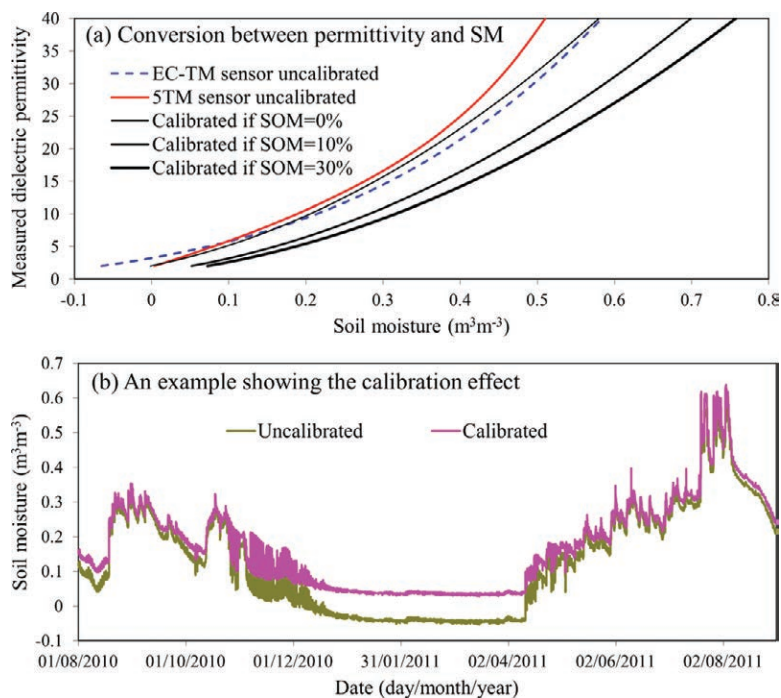


FIG. 2. (a) The calibrated conversion between the measured soil dielectric permittivity and SM, depending on volumetric SOC content; the default conversions for both EC-TM sensor and 5TM sensor are plotted for comparison. (b) An example (station 35 in Fig. 1c, with volumetric SOM content of 28% in the topsoil) to show the difference in EC-TM measured 0–5-cm SM before and after the calibration.

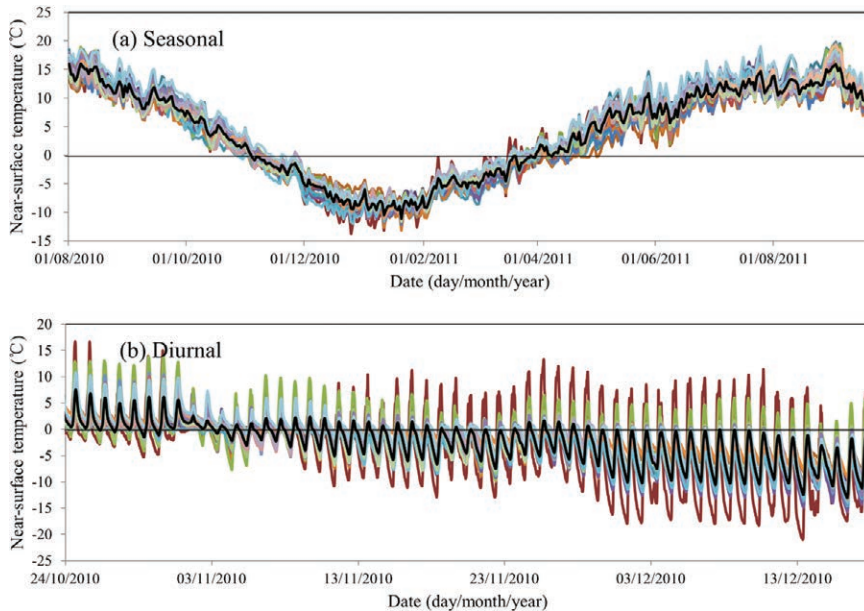


FIG. 3. (a) Seasonal variations of daily-mean soil temperature and (b) diurnal variations of freeze–thaw state, based on 0–5-cm observations at the 30 stations installed in 2010. The color lines denote the in situ observations at each station, and the thick black line denotes the station-averaged values.

layer at the 30 stations installed in 2010. It is shown that the annual range of daily-mean temperature is about 20°C and the spatial variability is less than 10°C. Figure 3b shows the diurnal F/T cycle for a specific period. We can see that the diurnal amplitudes of soil temperature are the smallest ones around the beginning of November, when the soil changes from diurnal F/T cycle into fully frozen state, indicating the water phase change releases a great deal of energy to delay the freezing process.

Figure 4 shows the observed seasonal and diurnal variations of near-surface (0–5 cm) SM at the 30 stations. The SM varies from 0.2 to 0.6 m³ m⁻³ in summer and from nearly 0 to 0.2 m³ m⁻³ in winter, showing a large spatial variability. This variability indicates that it is highly risky to use measurements at a single or few stations to evaluate SM products at a coarse resolution. Nevertheless, we find that the cross-

station correlation coefficient of SM time series is high ($R > 0.7$), indicating the SM time variability is dominated by precipitation events. The station-averaged SM also exhibits a high seasonal dynamics, increasing from 0.1 m³ m⁻³ in winter to 0.35 m³ m⁻³ in summer, confirming that this network is preferred for the validations of regional SM estimates. During the F/T cycle (Fig. 4b), SM has evident diurnal variations (high during days and low during nights).

Spatial upscaling of soil moisture. Because of the high spatial variability of SM, it is crucial to upscale point measurements to a coarse scale for regional studies. Crow et al. (2012) reviewed several spatial upscaling methods, but they are not readily applicable to a large-scale network (Qin et al. 2013). Here, we present the preliminary results of a time stability analysis and a new upscaling method based on the CTP-SMTMN data.

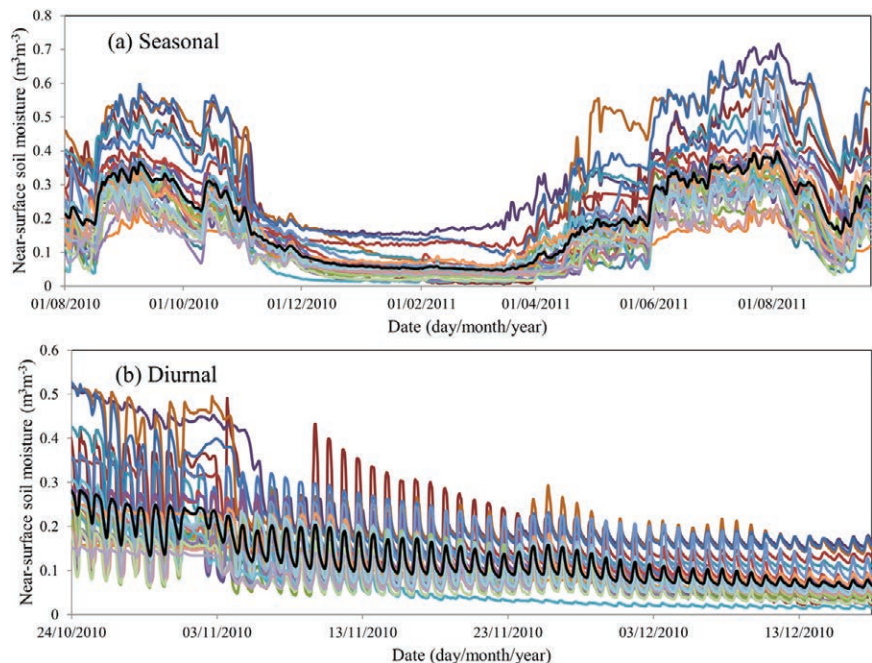


FIG. 4. As in Fig. 3, but for soil moisture.

Time stability analysis was first proposed by Vachaud et al. (1985), who found that it is possible to find a station to represent a region in terms of SM. Based on our network data, we find that the time stability is sensitive to soil wetness conditions, and none of the stations can represent the station-averaged SM in the large network for a full year, because the SM spatial distribution can be significantly changed by small-scale (~10 km) rainfall events and soil F/T cycle. Considering this issue, we proposed a method to estimate regional-mean SM by the combination of a few optimally selected stations that contain more information on SM spatial heterogeneity (Zhao et al. 2013). Figure 5a shows an example that the all-station-averaged SM in the large network is almost reproduced by a combination of five selected stations. In reality, we can find a number of station combinations that give equally robust estimates of regional SM, making it feasible and flexible to maintain the network at a relatively low cost.

Moreover, the network data have been used to support the development of a new SM upscaling approach (Qin et al. 2013). The essential idea is to introduce MODIS-derived apparent thermal inertia (ATI) as an extra data source to show the SM spatial variability. First, we develop a function to link the station-averaged SM and pixel-averaged ATI. Then, the function is used to estimate the area-averaged SM from ATI data at MODIS-pixel or larger scales. The estimated SM time series can reflect its temporal variations but is subjected to uncertainties as the function is empirical. Finally, we estimate the area-averaged SM at a targeted spatial scale by a weighted linear combination of station SM data. The weight coefficients are obtained through Bayesian

linear regression that minimizes the difference between the ATI-based SM estimate and the linear combination. As an example, Fig. 5b shows the spatial variation of JJA-averaged SM estimated from the upscaling approach. Figure 5c shows that the SM averaged over all the stations is very close to the upscaled one for the large network, indicating that the stations deployed along the cross transect have a reasonable representativeness for the large area.

Evaluation of SM products. The CTP-SMTMN can serve as a calibration/validation site for a number of remote sensing and land hydrological modeling products. For instance, the GLDAS outputs can be evaluated against the large and medium networks;

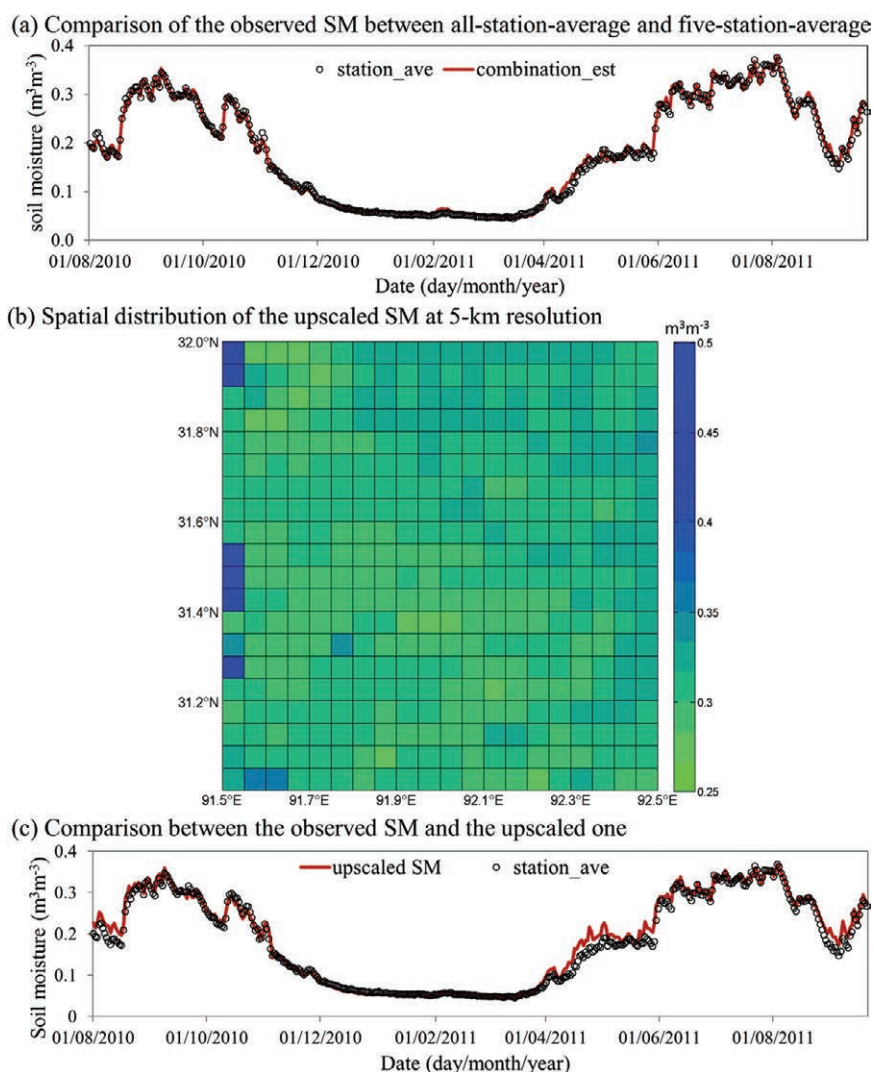


FIG. 5. (a) Comparison between the SM averaged over all the stations and the one averaged over five optimally selected stations (03, 10, 12, 22, and 28 in Fig. 1c) in the large network, (b) JJA-mean SM upscaled with the aid of MODIS ATI, and (c) comparison between the station-averaged SM and the upscaled one in the large network.

SM products retrieved from AMSR-E, SMOS, ASCAT, and SMAP can be evaluated against the medium network data; and the SM product from SMAP active signals can be compared with the small network data.

Figure 6 shows an example of comparing four SM products derived from AMSR-E ascending and descending signals with the upscaled SM in the large network. We find that the four satellite products have big biases against the observed SM in the semiarid area. Their root-mean-square error (RMSE) values range over 0.1–0.2 $\text{m}^3 \text{m}^{-3}$ for the monsoon season, similar to the results for two other satellite products evaluated by Su et al. (2011). Therefore, it is very challenging to estimate SM in this region, and current satellite products need substantial improvements (e.g., to consider the impact of high SOC content on the soil dielectric permittivity and to estimate soil surface temperature more accurately under the plateau environment) before used for basic research for the third pole.

DATA MANAGEMENT AND POLICY. We have completed major procedures, including network

design, sensor installation, data collection, sensor calibration, point-measurement upscaling, and data archive. All data have been quality controlled through checking SM time series one by one so as to remove suspected or wrong data. The metadata include station geographic position, elevation, slope, aspect, land cover, and soil texture, as well as SOC content, start time, and so on. They are prepared according to the International Soil Moisture Network (ISMN) required format for SM data and metadata.

To encourage the use of the network data by broad communities, we are cooperating with the ISMN (<http://ismn.geo.tuwien.ac.at/>) for publicizing the observed and scaled data. Of course, users can directly contact the authors for data access and more details. The recent 2-yr data is accessible online (see <http://dam.itpcas.ac.cn/rs/?q=data>), and follow-on data will be disseminated in due course, after a protection period of 1 year for the observers.

SUMMARY. We have established a multiscale soil moisture and temperature monitoring network in the central TP to support remote sensing, land modeling, and process studies for the third-pole region. The network

consists of 56 stations that measure soil moisture at three typical spatial scales. Up to October 2012, 30 stations have at least 2-yr data, 50 stations have at least 1-yr data, and another 6 stations have 4-month data. The network is running on a long-term basis and more data are expected to become available in the near future.

This network and the one established by Su et al. (2011) possess about 100 stations in total, which constitute the base of soil moisture and temperature observations on the third pole. By providing high-quality data, both networks would greatly contribute to the TPE program and international communities for quantifying the role of soil moisture and temperature in the multisphere interactions in this unique region.

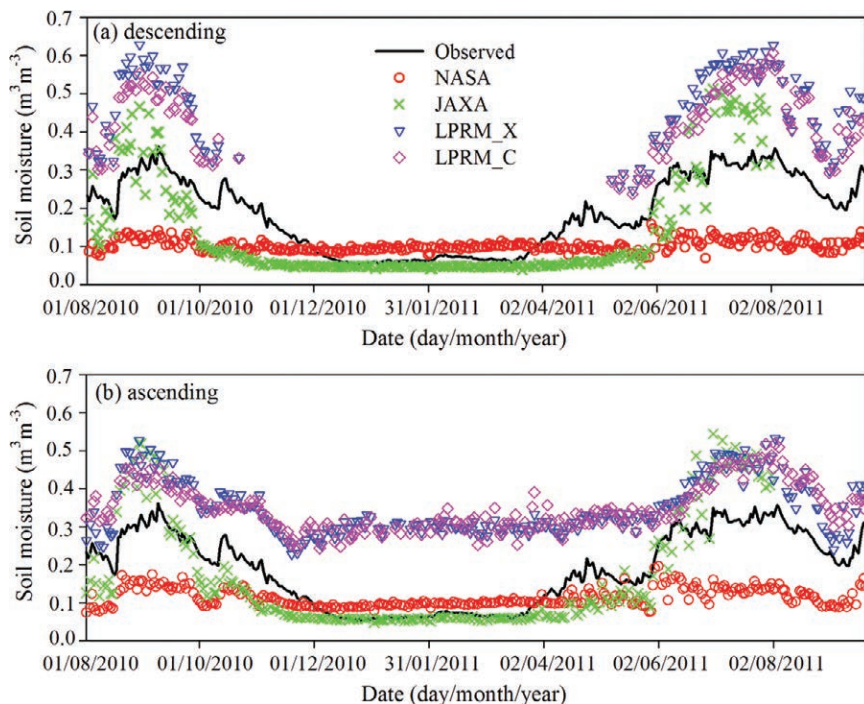


FIG. 6. Comparison between the upscaled SM and four AMSR-E SM products for the large-scale network area. (a) Products from AMSR-E descending data and (b) products from AMSR-E ascending data. The four products are from the National Aeronautics and Space Administration (NASA) (Njoku and Chan 2006), Japan Aerospace Exploration Agency (JAXA) (Koike et al. 2004), and Land Parameter Retrieval Model output based on C-band and X-band (LPRM_C and LPRM_X) (Owe et al. 2008)

ACKNOWLEDGMENTS. This work was financially supported by the Global Change Program of Ministry of Science and Technology of China Grant 2010CB951703, the CMA Special Fund for Scientific Research in the Public Interest Grant GYHY201206008, and the National Natural Science Foundation of China Grants 41190083 and EU-FP7 CEOP-AEGIS. The authors are greatly thankful to Drs. Toshio Koike (University of Tokyo), Bob Su (University of Twente), Tom Jackson (Hydrology and Remote Sensing Laboratory, USDA), Ichiro Kaihotsu (Hiroshima University), and Jeff Walker (Monash University) for their constructive suggestions to the network configuration as well as practical implementation.

REFERENCES

- Bartalis, Z., W. Wagner, V. Naeimi, S. Hasenauer, K. Scipal, H. Bonekamp, J. Figa, and C. Anderson, 2007: Initial soil moisture retrievals from the METOP-A Advanced Scatterometer (ASCAT). *Geophys. Res. Lett.*, **34**, L20401, doi:10.1029/2007GL031088.
- Chen, Y., K. Yang, W. Tang, J. Qin, and L. Zhao, 2012: Parameterizing soil organic carbon's impacts on soil porosity and thermal parameters for Eastern Tibet grasslands. *Sci. China Earth Sci.*, **55**, 1001–1011.
- Crow, W. T., and Coauthors, 2012: Upscaling sparse ground-based soil moisture observations for the validation of coarse-resolution satellite soil moisture products. *Rev. Geophys.*, **50**, RG2002, doi:10.1029/2011RG000372.
- Dorigo, W. A., and Coauthors, 2011: The International Soil Moisture Network: A data hosting facility for global in situ soil moisture measurements. *Hydrol. Earth Syst. Sci.*, **15**, 1675–1698.
- Entekhabi, D., and Coauthors, 2010: The Soil Moisture Active Passive (SMAP) mission. *Proc. IEEE*, **98**, 704–716.
- Fujii, H., and T. Koike, 2001: Development of a TRMM/TMI algorithm for precipitation in the Tibetan Plateau by considering effects of land surface emissivity. *J. Meteor. Soc. Japan*, **79**, 475–483.
- Gao, Z., N. Chae, J. Kim, J. Hong, T. Choi, and H. Lee, 2004: Modeling of surface energy partitioning, surface temperature, and soil wetness in the Tibetan prairie using the Simple Biosphere Model 2 (SiB2). *J. Geophys. Res.*, **109**, D06102, doi:10.1029/2003JD004089.
- Jacobsen, O. H., and P. Schjønning, 1993: A laboratory calibration of time domain reflectometry for soil water measurement including effects of bulk density and texture. *J. Hydrol.*, **151**, 147–157.
- Jin, R., X. Li, and T. Che, 2009: A decision tree algorithm for surface soil freeze/thaw classification over China using SSM/I brightness temperature. *Remote Sens. Environ.*, **113**, 2651–2660, doi:10.1016/j.rse.2009.08.003.
- Kawanishi, T., and Coauthors, 2003: The Advanced Microwave Scanning Radiometer for the Earth Observing System (AMSR-E), NASDA's contribution to the EOS for global energy and water cycle studies. *IEEE Trans. Geosci. Remote Sens.*, **41**, 184–194.
- Kerr, Y. H., P. Waldteufel, J. P. Wigneron, J. Martinuzzi, J. Font, and M. Berger, 2001: Soil moisture retrieval from space: The Soil Moisture and Ocean Salinity (SMOS) mission. *IEEE Trans. Geosci. Remote Sens.*, **39**, 1729–1735.
- Koike, T., Y. Nakamura, I. Kaihotsu, G. Davva, N. Matsuura, K. Tamagawa, and H. Fujii, 2004: Development of an Advanced Microwave Scanning Radiometer (AMSR-E) algorithm of soil moisture and vegetation water content. *Annu. J. Hydraul. Eng., Japan Soc. Civil Eng.*, **48**, 217–222.
- Li, X., and T. Koike, 2003: Frozen soil parameterization in SiB2 and its validation with GAME-Tibet observations. *Cold Reg. Sci. Technol.*, **36**, 165–182.
- , R. Jin, X. Pan, T. Zhang, and J. Guo, 2012: Changes in the near-surface soil freeze-thaw cycle on the Qinghai-Tibetan Plateau. *Int. J. Appl. Earth Obs.*, **17**, 33–42.
- Liu, J., Z. Sun, H. Liang, X. Xu, and P. Wu, 2005: Precipitable water vapor on the Tibetan Plateau estimated by GPS, water vapor radiometer, radiosonde, and numerical weather prediction analysis and its impact on the radiation budget. *J. Geophys. Res.*, **110**, D17106, doi:10.1029/2004JD005715.
- Lu, H., T. Koike, K. Yang, Z. Hu, X. Xu, M. Rasmy, D. Kuria, and K. Tamagawa, 2012: Improving land surface soil moisture and energy flux simulations over the Tibetan plateau by the assimilation of the microwave remote sensing data and the GCM output into a land surface model. *Int. J. Appl. Earth Obs. Geoinf.*, **17**, 43–54.
- Ma, Y., S. Kang, L. Zhu, B. Xu, L. Tian, and T. Yao, 2008: Tibetan Observation and Research Platform (TORP): Atmosphere–land interaction over a heterogeneous landscape. *Bull. Amer. Meteor. Soc.*, **89**, 1487–1492.
- Njoku, E., and S. Chan, 2006: Vegetation and surface roughness effects on AMSR-E land observations. *Remote Sens. Environ.*, **100**, 190–199.
- Oelke, C., and T. Zhang, 2007: Modeling the active-layer depth over the Tibetan Plateau. *Arct. Antarct. Alp. Res.*, **39**, 714–722.
- Owe, M., R. de Jeu, and T. Holmes, 2008: Multisensor historical climatology of satellite-derived global land surface moisture. *J. Geophys. Res.*, **113**, F01002, doi:10.1029/2007JF000769.

- Qin, J., K. Yang, N. Lu, Y. Chen, L. Zhao, and M. Han, 2013: Spatial upscaling of in-situ soil moisture measurements based on MODIS-derived apparent thermal inertia. *Remote Sens. Environ.*, **138**, 1–9.
- Qiu, J., 2008: The third pole. *Nature*, **454**, 393–396.
- Rasmy, M., T. Koike, S. Boussetta, H. Lu, and X. Li, 2011: Development of a satellite land data assimilation system coupled with a mesoscale model in the Tibetan Plateau. *Trans. Geosci. Remote Sens.*, **49**, 2847–2862.
- Robock, A., K. Y. Vinnikov, G. Srinivasan, J. K. Entin, S. E. Hollinger, N. A. Speranskaya, S. Liu, and A. Namkhai, 2000: The Global Soil Moisture Data Bank. *Bull. Amer. Meteor. Soc.*, **81**, 1281–1299.
- Rodell, M., and Coauthors, 2004: The Global Land Data Assimilation System. *Bull. Amer. Meteor. Soc.*, **85**, 381–394.
- Su, Z., J. Wen, L. Dente, R. van der Velde, L. Wang, Y. Ma, K. Yang, and Z. Hu, 2011: The Tibetan Plateau observatory of plateau scale soil moisture and soil temperature (Tibet-Obs) for quantifying uncertainties in coarse resolution satellite and model products. *Hydrol. Earth Syst. Sci.*, **15**, 2303–2316.
- Vachaud, G., A. Passerat De Silans, P. Balabanis, and M. Vauclin, 1985: Temporal stability of spatially measured soil water probability density function. *Soil Sci. Soc. Amer. J.*, **49**, 822–828.
- van der Velde, R., Z. Su, P. van Oevelen, J. Wen, Y. Ma, and M. S. Salama, 2012: Soil moisture mapping over the central part of the Tibetan Plateau using a series of ASAR WS images. *Remote Sens. Environ.*, **120**, 175–187.
- Wen, J., Z. Su, and Y. Ma, 2003: Determination of land surface temperature and soil moisture from Tropical Rainfall Measuring Mission/Microwave Imager remote sensing data. *J. Geophys. Res.*, **108**, 4038, doi:10.1029/2002JD002176.
- Xu, X., and Coauthors, 2008: A New Integrated Observational System over the Tibetan Plateau. *Bull. Amer. Meteor. Soc.*, **82**, 1492–1496.
- Yang, K., T. Koike, B. S. Ye, and L. Bastidas, 2005: Inverse analysis of the role of soil vertical heterogeneity in controlling surface soil state and energy partition. *J. Geophys. Res.*, **110**, D08101, doi:10.1029/2004JD005500.
- , T. Watanabe, T. Koike, X. Li, H. Fujii, K. Tamagawa, Y. Ma, and H. Ishikawa, 2007: Auto-calibration system developed to assimilate AMSR-E data into a land surface model for estimating soil moisture and the surface energy budget. *J. Meteor. Soc. Japan*, **85A**, 229–242.
- , B. Ye, D. Zhou, B. Wu, T. Foken, J. Qin, and Z. Zhou, 2011: Response of hydrological cycle to recent climate changes in the Tibetan Plateau. *Climatic Change*, **109**, 517–534.
- Yang, M., T. Yao, X. Gou, N. Hirose, H. Fujii, L. Hao, and D. F. Levia, 2007: Diurnal freeze/thaw cycles of the ground surface on the Tibetan Plateau. *Chin. Sci. Bull.*, **52**, 136–139.
- Yao, T., and Coauthors, 2012: Third Pole Environment (TPE). *Environ. Dev.*, **3**, 52–64.
- Zhang, R., T. Koike, X. Xu, Y. Ma, and K. Yang, 2012: A China-Japan cooperative JICA atmospheric observing network over the Tibetan Plateau (JICA/Tibet Project): An overview. *J. Meteor. Soc. Japan*, **90C**, 1–16.
- Zhang, T., and R. L. Armstrong, 2001: Soil freeze/thaw cycles over snow-free land detected by passive microwave remote sensing. *Geophys. Res. Lett.*, **28**, 763–766.
- Zhao, L., and Coauthors, 2013: Spatiotemporal analysis of soil moisture observations within a Tibetan mesoscale area and its implication to regional soil moisture measurements. *J. Hydrol.*, **482**, 92–104, doi:10.1016/j.jhydrol.2012.12.033.
- Zhao, T. J., L. X. Zhang, L. M. Jiang, S. J. Zhao, L. N. Chai, and R. Jin, 2011: A new soil freeze/thaw discriminant algorithm using AMSR-E passive microwave imagery. *Hydrol. Processes*, **25**, 1704–1716.

A MULTISCALE SOIL MOISTURE AND FREEZE–THAW MONITORING NETWORK ON THE THIRD POLE

BY KUN YANG, JUN QIN, LONG ZHAO, YINGYING CHEN, WENJUN TANG, MENGLEI HAN, LAZHU, ZHUOQI CHEN, NING LV, BAOHONG DING, HUI WU, AND CHANGGUI LIN

This document is a supplement to “A Multiscale Soil Moisture and Freeze–Thaw Monitoring Network on the Third Pole,” by Kun Yang, Jun Qin, Long Zhao, Yingying Chen, Wenjun Tang, Menglei Han, Lazhu, Zhuoqi Chen, Ning Lv, Baohong Ding, Hui Wu, and Changgui Lin (*Bull. Amer. Meteor. Soc.*, **94**, 1907–1916) • ©2013 American Meteorological Society • Corresponding author: Kun Yang, Dr., Prof., Institute of Tibetan Plateau Research, Chinese Academy of Sciences, Bldg 3, Courtyard 16, Lincui Rd., Chaoyang District, Beijing 100101, China • E-mail: yangk@itpcas.ac.cn • DOI:10.1175/BAMS-D-12-00203.2

TABLE ES1. The geographic location, slope, aspect, topsoil soil organic carbon (SOC) content, topsoil texture, and observation start date at each station of the three networks. “L,” “M,” and “S” denote a station in the large-, medium-, and small-scale network, respectively. Note that a few stations are shared by different networks.

Station code	Lon (°)	Lat (°)	Elevation (m)	Slope (°)	Aspect (°)	SOC (%)	Clay (%)	Silt (%)	Start date
L01	91.721	31.946	4637	0.3	214	2.0	3.5	34.5	1 Aug 2010
L02	91.700	31.890	4713	8.3	246	5.7	5.9	64.9	1 Aug 2010
L03	91.706	31.843	4799	2.3	228	1.8	5.1	38.4	1 Aug 2010
L04	91.750	31.806	4818	3.2	155	4.4	5.5	56.2	1 Aug 2010
L05	91.783	31.754	4723	2.8	166	4.9	7.3	54.9	1 Aug 2010
L06	91.811	31.722	4684	1.3	146	7.5	5.2	49.5	1 Jul 2011
L07	91.842	31.678	4628	3.7	120	2.4	9.6	59.4	1 Aug 2010
L08	91.795	31.662	4574	0.8	256	3.7	4.7	40.2	1 Aug 2010
L09	91.755	31.639	4570	6.2	274	2.9	5.9	46.7	1 Aug 2010
L10	91.740	31.614	4552	1.1	178	2.7	2.6	30.9	1 Aug 2010
L11	91.793	31.587	4539	0.5	15	4.1	8.0	60.9	1 Aug 2010
L12	91.913	31.574	4671	0.5	185	3.0	5.1	40.3	1 Aug 2010
L13	91.985	31.546	4574	2.1	69	3.2	8.8	57.7	1 Aug 2010
L14	92.050	31.527	4516	1.1	132	2.6	4.1	40.7	1 Aug 2010
L15	92.017	31.463	4537	1.3	225	2.3	8.1	48.0	1 Aug 2010
L16	91.971	31.410	4517	0.7	342	3.8	3.3	35.9	4 Jul 2011
L17	91.976	31.373	4559	3.3	37	1.2	6.4	37.8	17 Jun 2012
L18	92.041	31.332	4470	3.5	60	1.0	5.1	31.4	1 Aug 2010
L19	92.109	31.274	4478	4.1	259	5.0	6.2	45.6	1 Aug 2010
L20	92.164	31.232	4491	0.6	77	3.6	5.2	51.8	4 Jul 2011
L21	92.197	31.172	4548	3.6	24	2.9	4.7	45.9	1 Aug 2010
L22	92.250	31.128	4609	1.0	255	5.0	3.6	40.3	1 Aug 2010

TABLE ESI. Continued.

Station code	Lon (°)	Lat (°)	Elevation (m)	Slope (°)	Aspect (°)	SOC (%)	Clay (%)	Silt (%)	Start date
L23	92.309	31.107	4690	2.3	249	6.7	5.2	61.1	1 Aug 2010
L24	92.369	31.074	4835	4.3	222	20.8	2.5	47.8	3 Jul 2011
L25	92.458	31.713	4762	4.9	197	8.6	5.7	66.0	1 Aug 2010
L26	92.405	31.683	4612	5.2	234	9.7	5.8	58.0	1 Aug 2010
L27	92.342	31.664	4518	1.3	31	5.7	4.3	51.6	1 Aug 2010
L28	92.331	31.640	4491	3.7	195	13.0	3.1	44.0	3 Jul 2011
L29	92.241	31.587	4637	4.7	79	8.3	7.2	60.1	3 Jul 2011
L30	92.206	31.541	4769	6.8	69	1.5	4.0	50.8	1 Aug 2010
L31	92.133	31.496	4628	2.9	58	8.2	7.3	53.6	3 Jul 2011
L32	91.899	31.369	4505	0.4	276	1.4	4.9	36.4	1 Aug 2010
L33	91.848	31.301	4574	2.9	353	2.4	2.4	22.7	1 Aug 2010
L34	91.799	31.259	4630	3.6	241	2.4	5.1	48.5	1 Aug 2010
L35	91.760	31.175	4633	0.9	357	3.3	5.9	45.3	1 Aug 2010
L36	91.726	31.129	4765	3.0	285	1.6	6.2	45.1	1 Aug 2010
L37	91.688	31.089	4736	2.5	86	1.9	2.1	26.2	1 Aug 2010
L38	91.679	31.033	4675	1.3	260	2.8	3.9	44.3	1 Aug 2010
M01	91.730	31.782	4730	7.8	51	4.8	2.3	35.1	1 Jul 2011
M02	91.750	31.806	4818	3.2	155	4.4	5.5	56.2	1 Aug 2010
M03	91.796	31.816	4953	4.9	230	3.4	2.3	60.0	1 Jul 2011
M04	91.846	31.808	4804	5.8	164	7.7	1.6	38.3	1 Jul 2011
M05	91.725	31.743	4677	8.0	36	4.0	3.8	32.0	1 Jul 2011
M06	91.783	31.754	4723	2.8	166	4.9	7.3	54.9	1 Aug 2010
M07	91.766	31.732	4758	6.5	110	5.3	4.7	57.6	4 Jul 2011
M08	91.870	31.736	4665	1.0	143	2.7	3.8	49.9	1 Jul 2011
M09	91.719	31.685	4600	6.4	55	2.7	3.7	32.7	1 Jul 2011
M10	91.811	31.722	4684	1.3	146	7.5	5.2	49.5	1 Jul 2011
M11	91.771	31.683	4647	1.5	281	5.4	9.4	57.5	4 Jul 2011
M12	91.808	31.691	4672	4.1	170	11.1	4.4	54.1	1 Jul 2011
M13	91.842	31.678	4628	3.7	120	2.4	9.6	59.4	1 Aug 2010
M14	91.795	31.662	4574	0.8	256	3.7	4.7	40.2	1 Aug 2010
M15	91.904	31.671	4737	5.9	164	4.6	9.8	56.6	1 Jul 2011
M16	91.755	31.639	4570	6.2	274	2.9	5.9	46.7	1 Aug 2010
M17	91.740	31.614	4552	1.1	178	2.7	2.6	30.9	1 Aug 2010
M18	91.775	31.614	4585	3.7	60	4.2	3.8	38.6	4 Jul 2011
M19	91.841	31.618	4608	2.0	143	3.2	3.4	29.4	4 Jul 2011
M20	91.915	31.612	4780	6.3	172	4.0	9.6	56.0	4 Jul 2011
M21	91.793	31.587	4539	0.5	15	4.1	8.0	60.9	1 Aug 2010
M22	91.913	31.574	4671	0.5	185	3.0	5.1	40.3	1 Aug 2010
S01	91.766	31.732	4758	6.5	110	5.3	4.7	57.6	4 Jul 2011
S02	91.811	31.722	4684	1.3	146	7.5	5.2	49.5	1 Jul 2011
S03	91.802	31.716	4699	0.4	72	8.9	3.8	49.5	1 Sep 2012
S04	91.787	31.703	4697	3.1	3	8.2	3.9	53.2	2 Sep 2012
S05	91.774	31.698	4737	5.6	135	3.7	9.3	62.7	3 Sep 2012
S06	91.786	31.694	4719	6.7	209	6.8	4.5	63.7	4 Sep 2012
S07	91.799	31.693	4699	6.3	213	4.0	6.4	49.1	5 Sep 2012
S08	91.808	31.691	4672	4.1	170	11.1	4.4	54.1	1 Jul 2011
S09	91.771	31.683	4647	1.5	281	5.4	9.4	57.5	4 Jul 2011

TABLE ES2. The specification of 5TM and EC-TM capacitance probe of ECH₂O used in this network.	
Sensor dimensions	10 cm (l) × 3.2 cm (w) × 0.7 cm (d)
Sensor length	5.2 cm
Frequency	70 MHz
Apparent dielectric permittivity	
Range	1–80
Resolution	0.1 from 1 to 20; <0.75 from 20 to 80
Accuracy	±1 from 1 to 40 (soil range); ±15% from 40 to 80
Volumetric water content (VWC)	
Range	0%–100% VWC
Resolution	0.1% VWC
Accuracy	±0.02 m ³ m ⁻³ (using medium specific calibration)
Soil temperature	
Range	–40° to +50°C
Resolution	0.1°C
Accuracy	±1°C

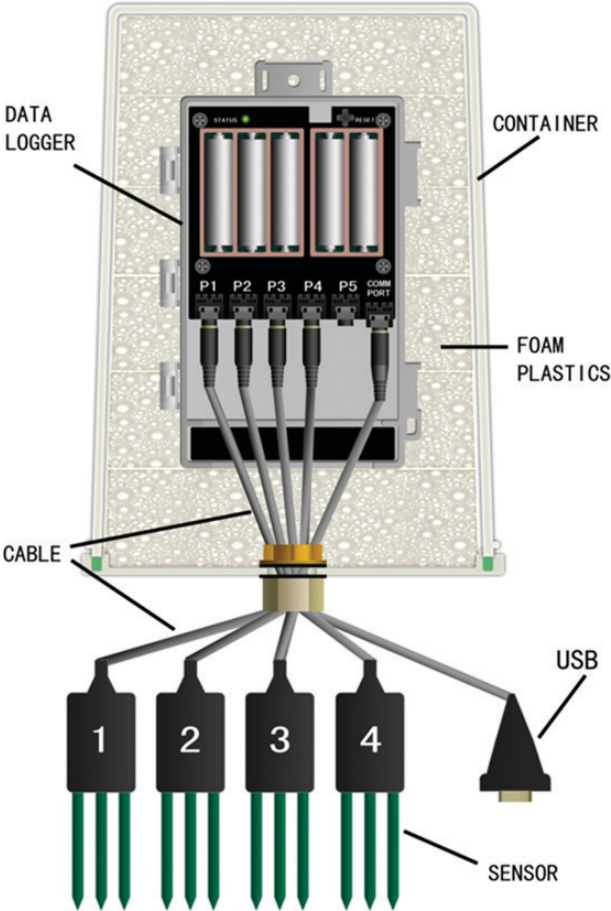


FIG. ES1. Schematic of the waterproof device used in the multiscale Soil Moisture and Temperature Monitoring Network on the central Tibetan Plain (TP-SMTMN) to protect the datalogger from damage by soil water intrusion. The device is composed of the container, the datalogger, and foam plastics in the space between the container and the logger. The device stands upside down within soils, with the opening of the container downward. Even if water gets through the hole on the opening into the container, it automatically seals the container and blocks air exchange between the inside and the outside. Further water intrusion increases the air pressure inside, which in turn resists the rising of the water level inside, according to the Clapeyron equation (the ideal gas law).